ELSEVIER

Contents lists available at ScienceDirect

Advances in Water Resources

journal homepage: www.elsevier.com/locate/advwatres



Root lateral interactions drive water uptake patterns under water limitation



Elizabeth Agee^{a,b,*}, Lingli He^a, Gautam Bisht^c, Valentin Couvreur^d, Parisa Shahbaz^a, Félicien Meunier^{e,f}, Christopher M. Gough[§], Ashley M. Matheny^h, Gil Bohrerⁱ, Valeriy Ivanov^{a,**}

- ^a Department of Civil and Environmental Engineering, University of Michigan, Ann Arbor, MI, USA
- ^b Environmental Sciences Division and Climate Change Science Institute, Oak Ridge National Laboratory, Oak Ridge, TN, USA
- c Atmospheric Sciences and Global Change Division, Pacific Northwest National Laboratory, Richland, WA, USA
- ^d Earth and Life Institute, Agronomy Department, University of Louvain, 1348 Louvain-la-Neuve, Belgium
- ^e Computational and Applied Vegetation Ecology, Department of Environment, Ghent University, Ghent, Belgium
- f Department of Earth and Environment, Boston University, Boston, MA, USA
- g Department of Biology, Virginia Commonwealth University, Richmond, VA, USA
- h Department of Geological Sciences, University of Texas at Austin, Austin, TX, USA
- ¹ Department of Civil, Environmental & Geodetic Engineering, Ohio State University, Columbus, OH, USA

ARTICLE INFO

Keywords: Root water uptake Root hydraulics Water stress Competition Lateral spread Rooting depth

ABSTRACT

The plasticity of root water uptake determines the maintenance of transpiration during periods of water limitation and drought. However, the mechanistic basis of plant water uptake, as well as the implications of water uptake strategies at the individual and ecosystem scale remain elusive. We model three-dimensional root water uptake under variably saturated conditions for a one-hectare temperate forest plot for a growing season with a pronounced mid-season dry period. Variations in root architecture, hydraulic properties, and degree of lateral interaction between root systems produce divergent local responses to water limitation and provide insights on individual and community response to meteorological conditions. Results demonstrate the plasticity of ecosystemscale responses to surface drying, where interacting roots shift regions of active uptake to deeper soil layers with less abundant root biomass. These shifts, a product of both root system and soil hydraulic properties, illustrate intimate links between root and soil hydraulics in determining plant water sourcing. We further demonstrate that root lateral interactions are beneficial at the ecosystem-scale, even when trees compete for water. Specifically, a more spatially extensive root system facilitates access to a larger soil water reservoir, often ameliorating water limitation and reducing sharp water potential gradients. While the reduction of water stress is a benefit, it can be offset by increased root construction and maintenance costs associated with the larger rooting system. A plausible "viability" region of root communal co-existence is therefore implied where competitive pressures and root production costs are balanced by a potential water benefit.

1. Introduction

Shifting patterns of precipitation and rising temperatures have highlighted forest vulnerability to heat- and drought-induced stresses. Water limitation conditions have been linked to decreases in forest productivity (Ciais et al., 2005; Zhao and Running, 2010), altered biogeochemistry (Schlesinger et al., 2016), increased rates of disturbance from fire, insect infestation, and disease (Kolb et al., 2016; Littell et al., 2016; Preisler et al., 2017), and, in extreme cases, mass tree mortality (Allen et al., 2010; Anderegg et al., 2016). While the impacts of prolonged water limitation are well understood, factors contributing to individual plant and community responses are nonlinear and difficult to disentangle (Phillips et al., 2016).

The subsurface, namely interactions between soils and root systems, is particularly complex, given variability in soil conditions (Fatichi et al., 2015a; Ivanov et al., 2010), root structure (Kramer-Walter et al., 2016; McCormack et al., 2017; Weemstra et al., 2016), and response patterns (He et al., 2014; Matheny et al., 2017a; Thomsen et al., 2013). Despite this complexity, there is consensus that improved understanding and model representation of subsurface dynamics is needed to fully describe water, energy, and ecological dynamics for vegetated ecosystems (McDowell et al., 2013). Over the past decade, there has been a unified effort to increase representation of root zone processes in models

^{*} Corresponding author.

^{**} Corresponding author.

across spatial scales and disciplinary foci (Couvreur et al., 2012; Manoli et al., 2014; Sulis et al., 2019). A number of reviews have highlighted current implementations of root system function and opportunities for improvement (e.g., Fatichi et al., 2015b; Javaux et al., 2013; Warren et al., 2015). Across scales, the majority of models rely on one-dimensional profiles of root biomass or length with depth, largely ignoring the lateral dimension of root mass and function. While pioneering studies have examined water uptake for overlapping root systems (e.g., Manoli et al., 2014), they typically examine a limited number of individuals with minimal representation of root topology or architecture.

For systems that face water-limitation, either from short-term, seasonal dry periods or longer-term droughts, plasticity of root water uptake (RWU) establishes the ability of individuals to meet atmospheric demand for moisture and maintain physiological function. The manifestion of plasticity is determined by both intrinsic properties of individuals and interactions within the community and environment. Of particular interest is how the spatial distribution of root structural and hydraulic properties contribute to the plasticity of RWU. Partitioning of root distribution or root niche separation, and stratified rooting depth may allow root systems to maintain adequate water supply during periods of water limitation (Brum et al., 2018; Ivanov et al., 2012; Silvertown et al., 2015). Rooting depth, in particular, is widely used in hydrological models to represent the region of plant-available moisture (Yang et al., 2016).

A proposed complement to vertical root segregation is the horizontal segregation of root systems –likely an equally crucial but less understood mechanism for efficient and thorough resource utilization (Schenk et al., 1999). The horizontal mingling of root systems is well-known, with studies of fine root competition and dynamics in monospecific and mixed-species forests finding strong support for overlapping root systems (Lang et al., 2010; Leuschner et al., 2001; Meinen et al., 2009; Valverde-Barrantes et al., 2015). While dependent on species and local environmental factors (e.g., soil and nutrient distribution), maximum root lateral extents have been observed as far as 20-40m from tree stem sources (Meinen et al., 2009; Stone and Kalisz, 1991), with Rewald and Leuschner (2009) reporting root lateral extents upwards of ten times beyond the tree crown radius. These extents all but guarantee lateral interaction between neighboring individuals.

Root system expansion, be it into deeper soil layers or laterally through surface soils, constitutes a significant investment in carbon through tissue construction and maintenance. Trade offs between carbon investment and the acquisition of critical resources (e.g., water and nutrients) forms the basis of plant economic theory, with potential competitive advantages conferred to those that optimize investment costs with resource gains (Bloom and Chapin, 1985). Approaches utilizing optimality theory have explored the balance between root zone investment and perceived acquisition benefits, garnering new insights into the distribution of plant rooting depths (Guswa, 2008; Yang et al., 2016) and soil moisture dynamics (Schymanski et al., 2008) across precipitation regimes. Yet, despite the ubiquitous co-mingling of lateral roots, the implications of investment in lateral root structure on water acquisition in natural forest ecosystems remains largely unaddressed.

Given inherent challenges to *in situ* measurement of below-ground processes, physically-based computational models of soil and root water dynamics provide an opportunity to explore and quantify the role of root spatial interactions *in silico* without the need for destructive field measurements. In this work, we introduce a computationally scalable model of three-dimensional RWU that captures forest plot-scale dynamics, including lateral interactions, while maintaining critical plant-scale structural and hydraulic information. We use observed field conditions during a typical growing season in a temperate, mixed-deciduous forest located in northern Michigan. The primary objective of this study is to explore and quantify the role of lateral root interactions in water uptake processes at the individual-tree and plot scales. Spatiotemporal patterns of water uptake, soil moisture, and plant water status were compared

for a range of root lateral spread scenarios, architectures, and hydraulic properties. Finally, we explore the implications that strategies of carbon investment in rooting structure may have on forest systems that experience water limitation.

2. Model theory

2.1. Root hydraulic architecture

2.1.1. Root system architecture

Root system architecture varies between and within species, with axes of variation arising from both physiological and environmental factors. Typically, system topology can be classified as one of three archetypes: flat (dominated by lateral roots near the surface, with secondary roots reaching deeper into the soil), tap (a dominant "carrot-like" vertical root with secondary roots sprouting laterally), or dimorphic (a mixed form of flat and tap root systems) (Sutton and Tinus, 1983). As technology to assess actual root architecture in field conditions without destructive measures (e.g., ground-penetrating radar) is still developing and unavailable for our study area, we use both flat and tap archetypes. While a given ecosystem may contain multiple topologies, each scenario in this study was assigned a single archetype. By choosing opposing topologies for comparison, we capture the range of potential root system configurations.

Three-dimensional root structures were generated using RootBox (v5e, available from https://www.csc.univie.ac.at/rootbox/) (Leitner et al., 2010), a dynamic root growth model that utilizes Lindenmayer-system (L-system) strings (Lindenmayer, 1977) to generate branching segments along predefined production rules. Production parameters were defined to generate two general root archetypes: tap and flat root systems (Supplementary Material S.1).

2.1.2. Hydraulic parameterization

Root hydraulic parameterization is accomplished through a hybrid macroscale approach (Couvreur et al. 2012, Meunier et al. 2017). The approach uses special cases of *microscale* RWU equations (Doussan et al., 2006) to generate *macroscale* parameters that are computationally tractable for large domain simulations, yet maintain microscale hydraulic information. Specifically, for each modeled root architecture, root segments are assigned intrinsic hydraulic conductivities that quantify the ease with which water flows from root surfaces to the stem.

Microscopic RWU is solved one time for two cases: (1) uniform and (2) hydrostatic soil water potential distribution with depth. From case (1), the relative contribution of each root segment to overall water uptake is determined and described as standard uptake fraction (SUF) by Couvreur et al. (2012). The SUF values depend on the specific root architecture and root hydraulic properties and are independent of the distribution of soil water potential or transpiration rate. Case (2) characterizes the root system's response to non-uniform soil water potential. The two cases yield whole root system equivalent conductance (K_{rs}) and the compensatory conductance (K_{comp}) . K_{comp} is a plant-scale parameter that quantifies the degree to which water uptake is locally enhanced in wetter soil regions and reduced in drier ones. When soil water potential is uniform, compensatory root water uptake is equal to zero. Similar to the SUF, K_{rs} and K_{comp} only depends on specific root architecture and hydraulic properties (Couvreur et al., 2012). Couvreur et al. (2012) also showed that for roots with high axial conductance, K_{rs} and K_{comp} can be approximated as equal. These plant- or macroscale quantities are further used in a coupled root and soil water physics model to simulate water uptake at a larger, plot-size scale. The Couvreur macroscopic parameterization scheme has been previously coupled to the R-SWMS (Couvreur et al., 2012, 2014), HYDRUS (Baram et al., 2016; Cai et al., 2018), and CLM models (Sulis et al., 2019).

2.2. PFLOTRAN-root water uptake

PFLOTRAN, a massively parallel flow and reactive transport model (Hammond et al., 2014; Lichtner et al., 2017), is used to solve the three-dimensional Richardson-Richards equation (Richards, 1931; Richardson, 1922) to describe flow in variably saturated soil. Root water uptake is described as a source/sink term in the Richards equation using the macroscale parameterization (Couvreur et al., 2012). The governing equation of the variably saturated flow mode in PFLOTRAN is given by

$$\frac{d \left(\rho \phi s\right)}{dt} = \nabla \cdot \left(\rho \frac{\kappa k_r}{\mu} \nabla (\varphi + \rho g z)\right) - S(x, y, z, t) \tag{1}$$

where ρ (kg m⁻³) is the density of water, φ (m³m⁻³) is soil porosity, s (-) is water saturation, κ (m²) is soil permeability, k_r (-) is relative permeability (-), μ (Pa s) is viscosity of water, φ (Pa) is soil water pressure and S (kg m⁻³ s⁻¹) is the sink or source due to root water uptake. In this work, we extended the variably saturated flow mode of PFLOTRAN to include macroscale RWU parameterization.

The domain is discretized into grid cells, represented as finite volumes with defined soil properties, hereafter referred to as soil grid cells. Multiple root systems may occupy the soil grid cell, each contributing to the overall uptake rate. At a soil grid cell, k, the total sink is expressed by Couvreur et al. (2012) as

$$S_{k,p} = T_{act, p} SSF_{k,p} + K_{comp,p} \left(H_{s,k} - \sum_{i=1}^{M} H_{s,i} SSF_{j,p} \right) SSF_{k,p}$$
 (2)

where $S_{k,p}$ is the generated sink term in the grid cell k for a root system p (p= 1, ... P); $T_{act,p}$ is the actual transpiration (or total uptake) for root system p; $H_{s,k}$ is the soil water potential of the grid cell k; M is the total number of soil grid cells that root system p occupies; K_{comp} is compensatory conductance (m^2 s^{-1}) and SSF is the standard sink fraction (-). $SSF_{k,p}$ is the aggregated value of standard uptake fractions (SUF) for all microscale root nodes (n=1, ..., N_k) occupying soil grid cell k,

$$SSF_{k,p} = \sum_{n=1}^{N_k} SUF_{n,k}.$$
 (3)

 K_{comp} and SUF are determined from macroscopic parameterization routines, specific to individual root systems, summarized in Section 2.1.2. The total sink for a grid cell k, S_k , is the sum of all water uptake rates from roots occupying the cell.

$$S_k = \sum_{p=1}^{P} S_{k,p} \tag{4}$$

Water potential at the root collar, H_{collar} , is used to determine the overall water potential status of the stem. H_{collar} is defined following Couvreur et al. (2012) as

$$H_{collar,p} = \sum_{j=1}^{M} H_{s,j} SSF_{j,p} - \frac{T_{act,p}}{K_{rs,p}}$$
 (5)

where $H_{collar,p}$ is the water potential at the root collar for root system p and K_{rs} is the whole root system equivalent conductance for root system p. A threshold water potential at the plant collar, H_{th} , is set as the hydraulic limit water uptake, mirroring isohydric stomatal response to water limitation. T_{act} is then expressed as a conditional function

$$T_{act,p} = \left\{ K_{rs} \left(\sum_{j=1}^{M} H_{s,j} SSF_j - H_{th,p} \right) if \left| H_{collar,p} \right| > \left| H_{th,p} \right| \right.$$

$$T_{pot,p} if \left| H_{collar,p} \right| < \left| H_{th,p} \right|$$

$$(6)$$

where $T_{pot, p}$ is tree-scale potential transpiration.

The open source repository for the PFLOTRAN-Root model is available through Github (DOI: 10.5281/zenodo.3540881).

Table 1

Allometric equations used to describe stem and root zone size characteristics. Equations describe tree height H (m), diameter at breast height DBH (cm), crown diameter W (m), crown height H' (m), stem fraction D (-), crown volume V (m³), and lateral spread LS (m).

Tree allometry Parameter	Equation	Reference					
Tree Height Crown Diameter Crown Height Crown Volume	$H = 9.97 \times \log [DBH] - 12.61$ $W = 2.67 \times \log [DBH] - 1.90$ $H' = D \bullet H$, where $D = 0.6$ $V = \frac{\pi}{6}H'W^2$	(Garrity et al., 2012) (Garrity et al., 2012) (Canham, 2005) Volume of an ellipsoid					
Scenarios of lateral spread							
Sc1, Localized Sc2, Intermediate Sc3, Extensive	LS = W/2 log [LS] = -0.202 + 0.406log [V] log [LS] = 0.2978 + 0.406log [V]						

3. Data and methods

3.1. Site description

This study uses data from the University of Michigan Biological Station in northern, lower Michigan, USA (45.56° N, 84.71° W). A temperate deciduous forest, the canopy is dominated by big-tooth aspen (*Populus grandidentata*) and paper birch (*Betula papyrifera*), with co-dominants and an understory consisting of red oak (*Quercus rubra*), maple (*Acer rubrum, Acer saccharum*), and pine (*Pinus strobes, Pinus resinous*). The mean annual precipitation is 805mm with a mean annual temperature of 6.8°C. Soils are well-drained Haplorthods of the Rubicon, Blue Lake or Cheboygan series with 92.2% sand, 6.5% silt and 0.6% clay (Nave et al., 2011). Meteorological, evapotranspiration, and soil moisture observations for the site are available through Ameriflux site ID US-UMB (Pastorello et al., 2020).

3.2. Tree size and allometry

During the 2011 growing season, a species-specific tree inventory was conducted within a 50m by 50m plot in the footprint of the US-UMB eddy covariance tower (He et al., 2014). This area serves as the domain for all subsequent analysis and model simulations. Spatial coordinates of all trees within the area were used to specify 'root collar' locations. Small trees (DBH ≤ 10cm) of the same species collocated within 2m of each other were assumed to share the same root system and aggregated to form a single stem. To prevent 'domain edge' effects, the computational area was expanded by 25m on all sides, with additional trees added at random following plot derived distributions of stem density and size. The entire computational domain is thus 100m x 100m x 2m and contains 574 trees with DBH values ranging from 5 to 73.5cm. Site-specific allometric relationships from previous studies were used to approximate tree height, crown diameter, and crown height (Table 1, Garrity et al., 2012). Crowns were assumed to be ellipsoids for the purpose of determining their volume. This information was used to generate time series of tree potential transpiration.

3.3. Forcing data

Time varying boundary conditions, specifically net precipitation and potential transpiration (T_{pot}), were generated for a subset of the 2010 growing season (06/07/2010 – 08/23/2010) (Fig. 1c) using tRIBS+VEGGIE (Ivanov et al., 2008), an ecohydrological model that represents water and energy processes and essential regulatory processes for vegetation. Specifically, ecosystem scale T_{pot} was determined by imposing ample soil moisture conditions to ensure that water uptake was never constrained. T_{pot} was downscaled to individuals in proportion to their crown volume and fraction of root system that resided within the

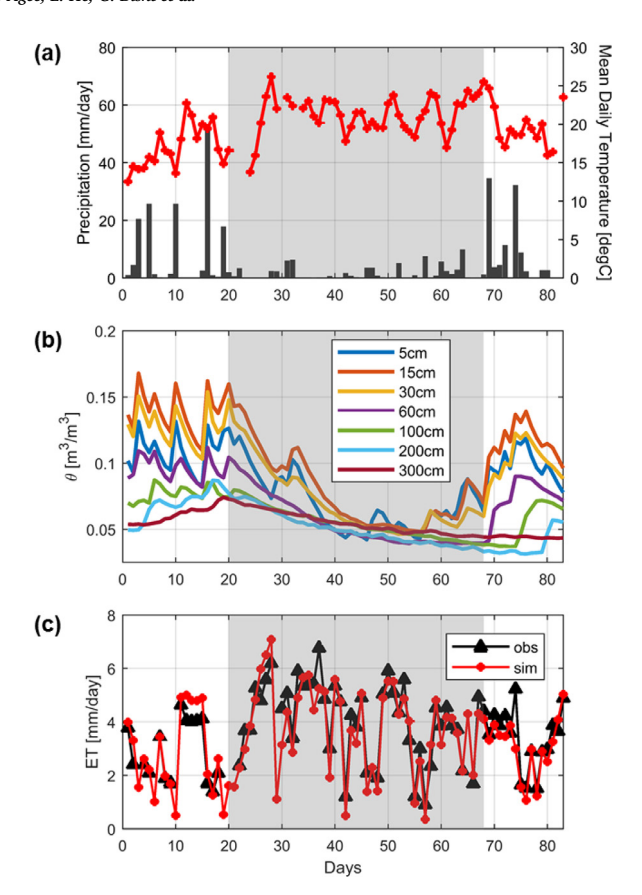


Fig. 1. Site conditions and forcing for the simulation period 06/07/2010 – 08/23/2010. (a) Precipitation and mean daily temperature, (b) observed soil water content from different depths near the US-UMB tower, and (c) observed evapotranspiration and potential evapotranspiration as generated from tRIBS+VEGGIE. The gray shaded region denotes a dry period where soil moisture values began declining.

100m x 100m plot,

$$T_{pot,p} = T_{pot} A \frac{F_{root,p} V_p}{\sum_{p=1}^{N} F_{root,p} V_p}, \tag{7}$$

where $T_{pot,p}$ is the potential transpiration for stem p (kg s⁻¹), T_{pot} is the ecosystem scale potential transpiration per unit area (kg s⁻¹ m⁻²), A is the simulation domain area (m²), $F_{root,p}$ is the fraction of root system p that resides within the simulation domain (-), and V_p is the crown volume of stem p (m³).

Simulated net precipitation, the difference between measured total precipitation and losses due to interception processes, is uniformly distributed throughout the domain. Horizontal homogeneity of precipitation is a simplification of actual conditions, where interception and throughfall processes may produce highly heterogeneous patterns of soil water infiltration. This simplification was chosen for the purpose of this numerical exercise to isolate the effects of root system architecture and lateral interaction on water uptake patterns.

3.4. Soil hydraulic properties

Soil saturation and pressure were characterized using Mualem-van Genuchten (MVG) soil characteristic curves (van Genuchten, 1980; Mualem, 1976). Parameters defining the shape of the curve were taken from He et al. (2014) and derived from Rajkai and Várallyay (1992) to define soil water retention and hydraulic conductivity curves. The two soil parameter sets represent potential conditions for the observed soil composition (Table 2, Supplementary Material S2).

Table 2
Soil hydraulic parameters used to define the van Genuchten (1980) soil water and hydraulic conductivity curves. Soil 1 properties were taken from He et al. (2014) and soil 2 properties were derived from Rajkai and Várallyay (1992).

Soil hydraulic properties Parameter	Soil 1	Soil 2	Unit
K_s , Saturated hydraulic conductivity θ_s , Saturated volumetric soil moisture content θ_r , Residual volumetric soil moisture content α , Shape parameter of van Genuchten (1980) n , Shape parameter of van Genuchten (1980)	350 0.3700 0.0400 0.0052 1.68	350 0.4856 0.0056 0.0029 1.38	mm h ⁻¹ m ³ m ⁻³ m ³ m ⁻³ mm ⁻¹

3.5. Root distributions and zones of uptake

Modeled root architectures rely upon inference from measured root structural information, in particular, root length. Root length density (RLD) is used to describe the length of root per soil volume. RLD does not linearly scale with the more commonly measured root biomass and requires additional information for conversion, including root diameter distribution (Fig. 2a). Root biomass density (RBD) was quantified at 20cm intervals to a soil depth of 80cm using cores sampled near the US-UMB tower (He et al. 2013). The median dry weight root mass by depth was fitted to an exponential decay function, given by $RBD(z) = 5478.8 \exp(-0.038 z)$ where z is depth (cm). The broad spatial distribution of root sampling throughout the inventoried plot was intended to capture the range of system-wide (rather than individual tree). Specific root length (SRL), the ratio of root dry mass to root length, was measured for root diameters ≤ 2mm. Root length and diameter were estimated using the WinRhizo software (Regent Instruments, Canada). Fine root distribution was divided into four diameter classes (0-0.05 mm, 0.05-0.1mm, 0.1-0.15mm, and 1.5-2.0mm) based on fractions reported for similar temperate forest sites (Makita et al., 2009; Montagnoli et al., 2012). The RLD profile is described as

$$RLD(z) = \sum_{c=1}^{C} f_c RBD(z) SRL_c$$
 (8)

where RBD(z) is root biomass density (g m $^{-3}$) as a function of depth z, SRL is specific root length for diameter class c (m g $^{-1}$), f is the fractional percentage of diameter class i, and C=4 is the number of root diameter classes.

3.6. Lateral spread scenarios

Three scenarios of lateral spread were designed to examine the relationship between root spatial interactions and tree water status (Fig. 3). Scenario 1 (Sc1 or *localized*) acts as a 'lower bound' for root lateral spread, in which the root system extent mirrors the extent of the aboveground crown projection. Scenarios 2 and 3 (Sc2 and Sc3 or *intermediate* and *extensive*) utilize the lower and upper confidence intervals for root allometric relationships for semi-humid environments from Casper et al. (2003), with lateral spread a function of crown volume (Fig. 3b). While the coarse architecture of the root systems expand, fine roots are spatially redistributed, weighted by individual size, such that each scenario maintains the same median root length density profile (Fig. 2b and Fig. 4).

3.7. Root competition index

Tree size is frequently used to extrapolate system scale behavior from local measurements. While size plays a large role in determining the area from which individuals acquire water and nutrients, it does not account for competition from neighboring individuals. To account for both system size and spatial interactions, we adapted analogous above-ground competition metrics (Arney, 1973) to develop a Root Competition Index

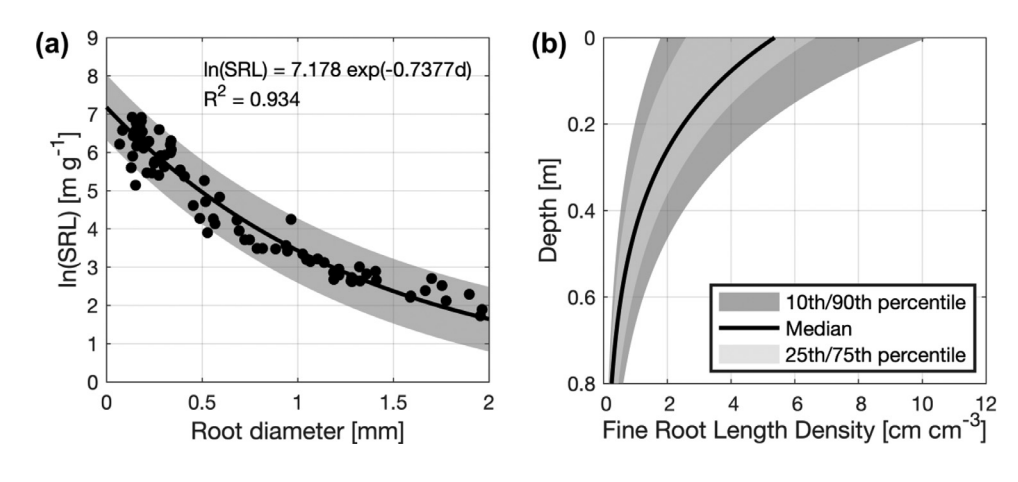


Fig. 2. (a) Empirical relationship between SRL and fine root diameter fitted to the function $\ln(\text{SRL})=7.178$ exp(-0.7337*d*), with $R^2=0.9340$, given as a black line with 90% confidence intervals in gray. (b) The calculated vertical profile of RLD for the US-UMB plot. The dark gray shaded region encompasses the $10^{\text{th}}-90^{\text{th}}$ percentiles, the light shaded region encompasses the $25^{\text{th}}-75^{\text{th}}$ percentiles, and the black line is the median.

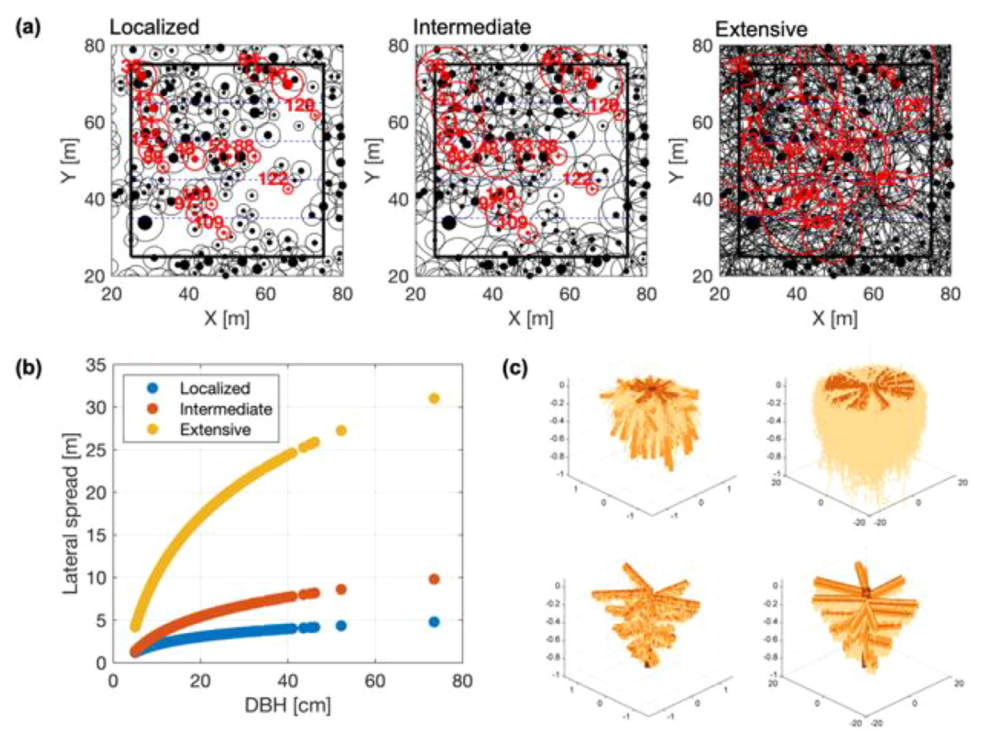


Fig. 3. (a) Three scenarios of lateral spread with an increasing degree of interactions from left to right. Black filled circles mark stem locations with marker size proportional to DBH and black circles denote individual lateral spread. Representative individuals (Section 3.8) are marked in red. Figure depicts a subset of the simulation domain for clarity; see SM for full simulation domain. (b) Relationship between DBH and root lateral spread as given in Table 1. (c) Root architectures generated with the Root-Box model (flat and tap root archetypes) for lateral spreads of 1m and 20m, with fixed maximum rooting depth of approximately 80cm (fourth and fifth branching order roots are not shown). (For interpretation of the references to color in this figure legend, the reader is referred to the web version of this article.)

(RCI). The RCI is given by

$$RCI_i = 100 \left(\frac{\sum_{j=1}^{n} a_{ij} + RA_i}{RA_i} \right)$$

$$(9)$$

where a_{ij} is the area of root zone overlap between subject tree i and competitor j, RA_i is plan area of root system i, and n is the number of competitors as defined by area overlap. An RCI value of 100 indicates zero interaction between root systems.

To characterize the impact of lateral interaction on water uptake and water potential status, representative individuals were selected using k-means cluster analysis (Lloyd, 1982). The selection of cluster variables was an attempt to balance changes in root overlap with differences in demand due to tree size. Specifically, for each lateral spread scenario, clusters (k=4) were obtained according to RCI and DBH. First, each cluster partition was assigned a value (1-4) that weighted its degree of interaction *relative* to the other partitions (based on RCI). For example, a cluster value of 1 would indicate low spatial interaction relative to the other clusters, while a value of 4 would indicate a high degree of spatial interaction relative to the other clusters. The assigned cluster values for each individual was summed across the three lateral spread scenarios to determine an aggregate rank, with values ranging 3-12. The aggregate

rank accounts for nonlinear changes in root system interaction areas across Sc1-Sc3 and unites them under one metric.

The aggregate rank is a measure of relative competition status but does not fully account for differences in demand based on tree size. Therefore, cluster analysis was repeated for the aggregate rank and DBH. Randomly selected individuals from each cluster were used for further analysis.

3.9. Quantifying carbon-water tradeoffs

Several metrics were used to quantify individual root structural investment and response to water limitation. Relative carbon investment in root structure between the scenarios was quantified for fine roots and coarse roots for each modeled individual. Relative carbon investment, C, for a root system p can be described as:

$$C_p = \frac{L_p - L_{min}}{L_{max} - L_{min}} \tag{10}$$

where L_p is the total root length for root system p, L_{min} is the minimum total root length from all individuals within the simulation domain, and L_{max} is the maximum total length from all individuals within the

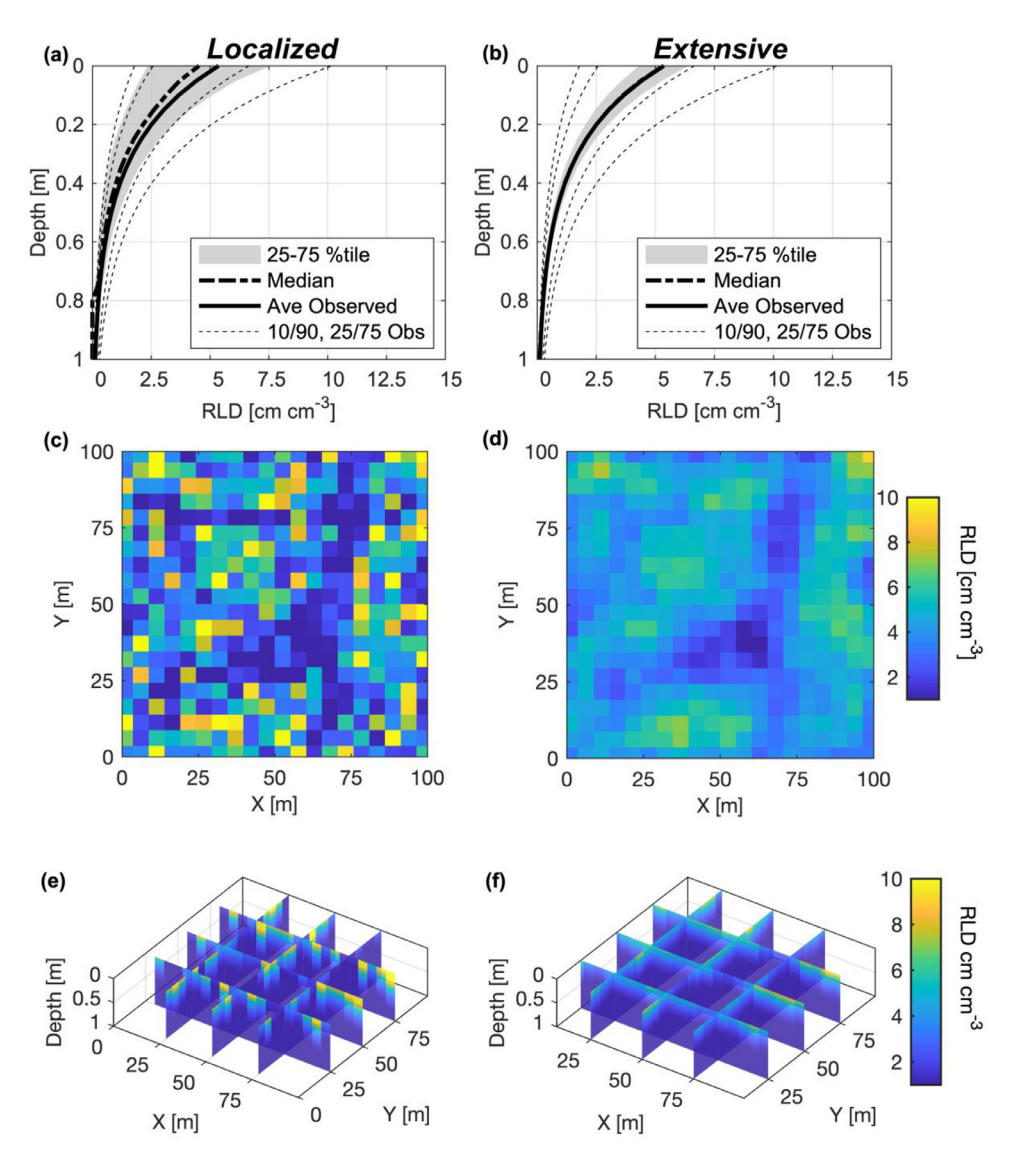


Fig. 4. Illustration of distributions for the *localized* (Sc1) (a, c, e) and *extensive* (Sc3) (b, d, f) rooting scenarios. (a – b) Domain scale RLD for the extrema scenarios with the simulated median (black dashed line) and 25-75th percentile range (shaded gray) shown against the observed profile percentiles (10^{th} , 25^{th} , 75^{th} , and 90^{th} in light gray dashes; average profile is the black solid line). (c – d) Areal view of 90^{th} percentile RLD at $5m \times 5m$ scale. (e – f) 3D domain slices showing RLD with depth across simulation domain at 0.05m depth scale. Color scales are uniform across (c – f).

simulation domain, across all lateral spread scenarios. The relative carbon investment was computed separately for coarse roots and fine roots.

Days where potential demand was not met (i.e., $T_{act} < T_{pot}$) were counted across the simulation period and compared between the scenarios. These are referred to as 'soil controlled days' as dry soils impede the individual's ability to meet atmospheric moisture demands. As lateral spread increases, the volume of the soil water reservoir also increases, at the cost of increased interaction. The 'cost of cooperation', W, quantifies the relative water benefit conferred upon an individual for expansion of the root system and is analogous to an aridity index. It is computed for an individual root system p as

$$W_p = 1 - \frac{T_{act,p}}{T_{pot,p}} \tag{11}$$

where T_{act} is determined following Eq. (6) and T_{pot} following Eq. (7). A value of 0 indicates that all potential demand is met, while a value of 1 indicates that no water uptake occurs. Beyond a simple aridity index, Wp is a measure of the cost of cooperation across root scenarios when all other abiotic facts (e.g., soil, climate) are held constant. Beyond a simple aridity index, Wp is a measure of the cost of cooperation across root scenarios when all other abiotic facts (e.g., soil, climate) are held constant.

Additionally, the centroid of root water uptake characterizes the "center of mass" of the moisture sink density distribution due to an indi-

vidual's transpiration flux. When the moisture sink density distribution is proportional to the root length density distribution, the centroid of uptake will occur at the root distribution's center of mass (0.385m for the distribution illustrated in Fig. 2b). A shift of the centroid above the center of mass indicates that roots in shallow layers are contributing proportionately more to uptake than deeper roots. The opposite is true when the centroid shifts below the root distribution center of mass. To compare shifts across the different scenarios with variable magnitudes of cumulative uptake, each individual's centroid was weighted by its daily water uptake.

4. Results

4.1. Degree of root interaction

The three rooting scenarios produced a wide range of root interaction. Lateral spread ranged from 1.2-4.8m, 1.3-9.8m, and 4.2-31.0m for the *localized, intermediate*, and *extensive* scenarios, respectively. The RCI ranged from 100-477, 100-834, and 2784-5479 across the rooting scenarios (Supplemental Material, Fig. S11). A value of 100 indicates no root system overlap and was found in both the *localized* (Sc1) and *intermediate* (Sc2) rooting scenarios. The largest degree of interaction occurred within the northwest quadrant of the analysis domain (Fig. 5c)

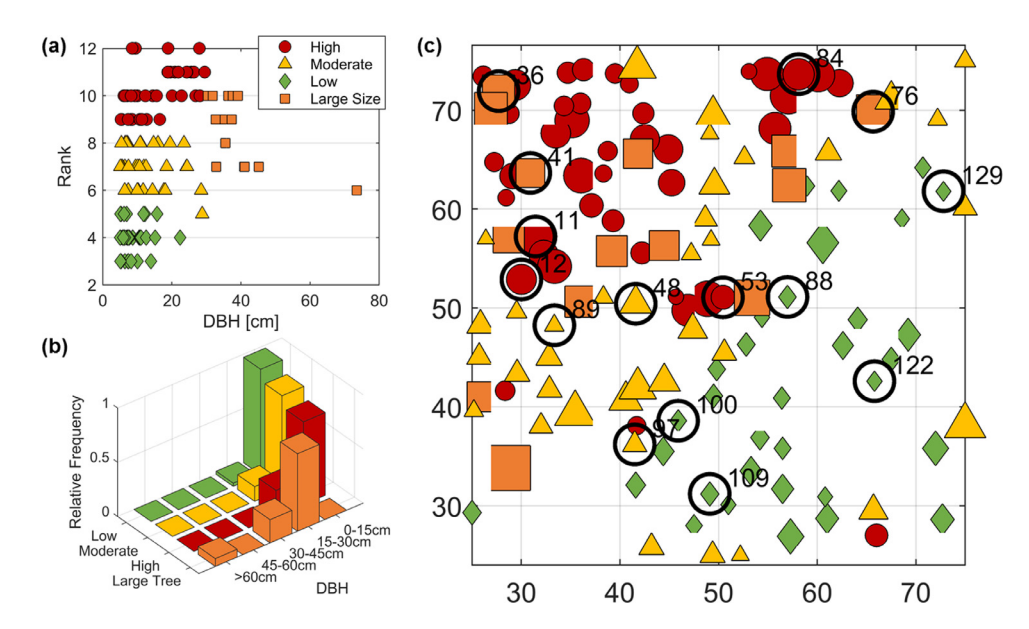


Fig. 5. (a) K-means cluster analysis for all 127 individuals of the inner 50m x 50m plots based on aggregate rank and DBH. (b) Relative frequency per size class for each representative group. (c) Representative groups within the simulation domain, with randomly selected individuals marked by black circles and their simulation identifier. In all plots, groups are represented as *low interaction* (green diamonds), *moderate interaction* (yellow triangles), *high interaction* (red circles), and *large size* (orange squares). (For interpretation of the references to color in this figure legend, the reader is referred to the web version of this article.)

which consisted of primarily large growth trees with a higher relative stem density.

Cluster analysis identified four major groups based on root competition and tree size. The four groups were labeled: *low interaction, moderate interaction, high interaction*, and *large trees* (Fig. 5a-b). The three "interaction" groups encompass individuals with DBH \leq 30cm binned according to rank. These clusters have ranks ranging from 3-5, 5-8, and 9-12, respectively. The *large tree* cluster encompasses individuals with DBH \geq 30cm spanning the *moderate* and *high interaction* levels, with ranks ranging from 6-10. Representative individuals from each cluster (n=3-5) were randomly selected and used in the subsequent analysis (Fig. 5c, Table S5).

4.2. Magnitude of water uptake

The growing season was marked by consistent rainfall events until simulation day 22 when precipitation events decreased in magnitude and frequency (Fig. 1a). The mid-season dry period ended on day 68, when more frequent precipitation resumed. A comparison of eddy-covariance measured latent heat fluxes with modeled domain scale T_{pot} indicate that despite relative soil dryness, observed T_{act} was not constrained (Fig. 1c), with a cumulative total of 281mm over the period.

For the modeled systems, the relationship between T_{pot} and T_{act} was driven by soil hydraulic properties and rooting scenario. Under Soil 1, simulated T_{act} does not meet T_{pot} due to excessive drying of the soil across the scenarios (Fig. 6a). As root lateral spread increases, accessible soil water reservoirs grow, increasing system wide cumulative uptake, T_{act} , from 183 to 233mm. For Soil 2, which had higher porosity and overall soil water content, uptake was not as constrained and T_{pot} was met across all three scenarios. The difference in RWU between Soils 1 and 2, which were derived using the same soil textural information (Supplemental Material S2) indicates a strong control of soil hydraulic parameterization over RWU and the onset of water limitation, decoupled from root hydraulic parameterization.

The influence of root structural archetype (e.g., flat roots vs. tap roots) was examined across all lateral spread scenarios. For individuals, the cumulative difference in RWU across the growing season varied from 0-11.2% and 0-4.5% for the *localized* (Sc1) and *extensive* (Sc3) lateral spreads respectively (see Supplemental Material S6 for individual breakdown). Averaged across the representative groups, differences were most pronounced for *large trees* with *localized* roots (Table 3, Large Trees) and to a lesser extent, those experiencing high relative competition (Table 3, High Interaction). Given the similarity between the two

architecture responses, all subsequent results and discussion will refer to the flat root structural archetype, unless otherwise noted.

While system wide water uptake increases with root lateral expansion, the effects differ among interaction groups (Fig. 6b-d). For the *extensive* rooting scenario (Sc3), periods of water stress, as indicated by the number of "soil controlled days," increase for the *low interaction* group, stay relatively the same for the *moderate interaction* group, and decrease for the *high interaction* and *large tree* groups (Fig. 6b). Mean diurnal uptake increases for the *high interaction* and *large tree* groups (Fig. 6c-d), with these groups contributing the bulk to system wide increases in cumulative water uptake (Fig. 6a-d).

4.3. Shifting zones of water uptake

Under water limitation (Soil 1), individual uptake during the midperiod shifts away from the root system's center of mass into deeper soil layers (Fig. 7, left panel). The centroid of RWU responds quickly to small pulses of rainfall, returning to the center of root mass distribution or to surface layers as water percolates through the soil column. The midperiod rainfall events were not large enough to saturate the entire soil column, with the centroid returning to deeper layers as the rainfall pulse was depleted. As lateral interaction increases, the magnitude and timing of centroid shifts change across all representative groups. Dense areas of the forest (i.e., areas of moderate and high interaction) and large trees experience larger downward shifts in the centroid of uptake relative to less dense areas of low interaction. As root lateral spread becomes more extensive, the low interaction group experiences a downward shift of the centroid, indicating shallow soil drying and higher competitive stress. Across all groups, the onset of deeper uptake occurs earlier in the dry period (days 23-35) for the localized scenario compared to the extensive scenario, where uptake shifts around day 33. While the shifts in RWU occur later and are shorter for extensive rooting, they are more intense, with deeper uptake occurring across all representative groups. Without water limitation (Soil 2, Fig. 7, right panel), there are no significant shifts away from the center of root mass distribution.

At the plot scale, water uptake from characteristic wet (days 22-26) and dry (days 34-38) periods were compared for four soil layers (Fig. 8). During the well-watered period, the relative contribution of different soil layers to domain-scale RWU is fairly consistent, mirroring the root length density distribution. However, as these layers dry and water limitation sets in, the relative contribution of deeper soil layers (specifically, 40-60cm and 60-80cm) increases by 10-15%. These shifts are seen across all lateral interaction scenarios, but at varying intensity.

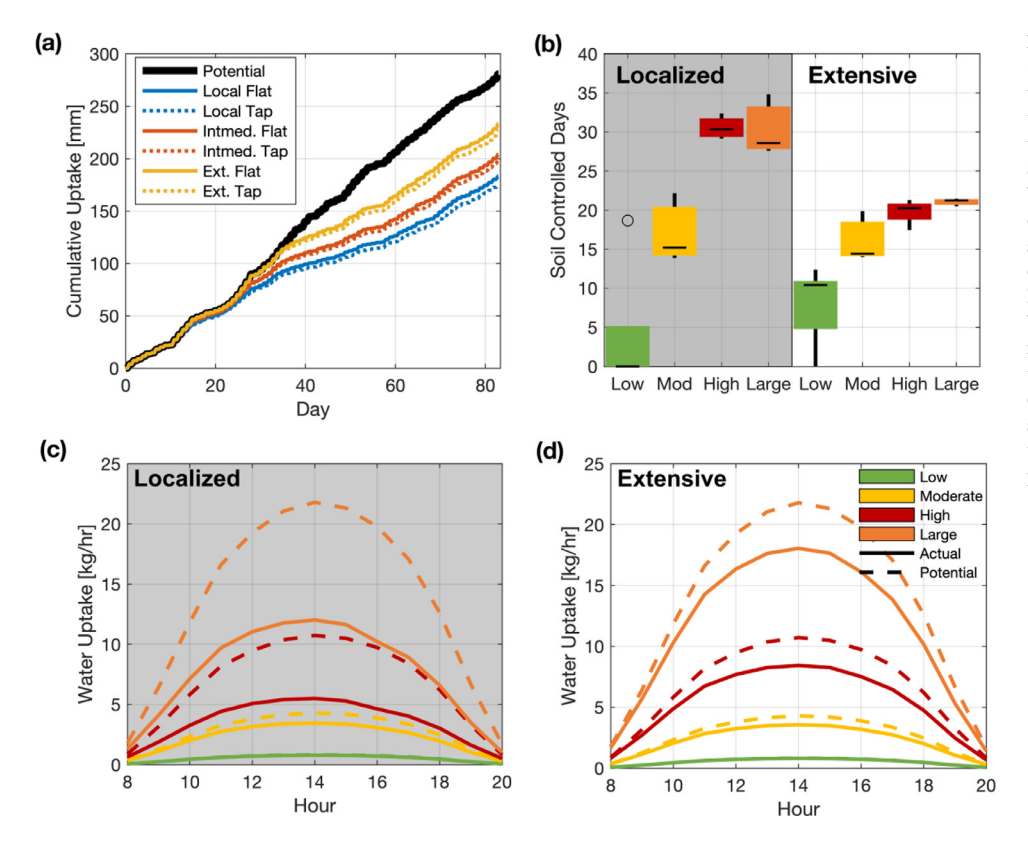


Fig. 6. (a) Cumulative system-scale uptake (mm) for Sc1-Sc3 under water-limited conditions (Soil 1, colored lines). Cumulative uptake for Soil 2 was equal to the potential transpiration (black solid line). Root structural archetype and lateral spread scenario is given by the legend. (b) Number of days during which dry soil limited water uptake for the representative clusters for low to large interaction classes. Quartile ranges are given by the box length, range by the whisker, median by the black interior line, and outlier by the open marker. (c - d) Mean daily uptake (kg hr-1) for the localized (Sc1) and extensive (Sc3) rooting extents. Solid lines represent the actual transpiration while dashed lines represent potential transpiration. The color scheme follows the presentation in panel (b).

Table 3Mean percent difference of cumulative uptake between flat roots and tap roots for the extrema lateral spread scenarios (*localized* and *extensive*).

Classification	Mean Localized, Sc1	Std	Mean Extensive, Sc3	Std
Low Interaction	-2.29	4.48	-0.53	0.64
Moderate Interaction	-0.47	0.17	-0.75	0.65
High Interaction	-1.01	0.12	1.76	1.39
Large Tree	6.44	1.03	1.20	1.36

4.4. Soil moisture

Mean soil water content in the root zone (top 80 cm) decreased from $0.20~\text{m}^3~\text{m}^{-3}$ in the early growing season, to $\leq 0.10~\text{m}^3~\text{m}^{-3}$ in the mid-season dry period. As rain events became more frequent, mean water content rose above 0.10 m³ m⁻³. Mean soil water content values were comparatively lower during the dry period for the extensive rooting scenario (Sc3), indicative of the higher rates of cumulative uptake (Fig. 9a, b). During the dry period, spatial patterns of soil moisture closely track root system distributions (Fig. 9c, d), with localized roots (Sc1) displaying higher spatial heterogeneity than extensive roots (Sc3). This is especially apparent when examining the coefficient of variation (Cv) of root zone soil water potential across the simulation period (Fig. 9e). The localized (Sc1) and intermediate (Sc2) rooting scenarios, with similar root density distributions show similar patterns of Cv, with values exceeding 1 during the dry period. Cv for extensive (Sc3) rooting is lower, never exceeding 1, even during the mid-season dry period, implying a relatively higher homogeneity in the spatial distribution of root zone soil water. For comparison, the Cv of RLD is 1.25, 1.07, and 0.95 for the localized, intermediate, and extensive rooting scenarios respectively. During periods of high precipitation, the Cv of SWP is lower than the Cv of RLD. As soil reservoirs are depleted during the dry period, the Cvof SWP approaches or exceeds the Cv of RLD. These periods of higher variability in soil water potential compared to root density may arise from the interplay between local root hydraulic properties and individual uptake demands. Overall, these results highlight two complementary processes: mean soil moisture behavior and variability of soil moisture. As mean water content decreases in Sc3 relative to Sc1 (i.e., $\bar{\theta}_{Sc3} < \bar{\theta}_{Sc1}$), spatial variability of soil water content as decreases (i.e., $Cv_{Sc3} < Cv_{Sc1}$).

4.5. Carbon investment vs. water acquisition

Median plot-scale fine root density was the same across all tested scenarios (Fig. 4a-b). With increasing lateral spread, fine roots were distributed proportionately across coarse structural roots. As such, relative fine root carbon costs remained relatively consistent between all three scenarios (Fig. 10a). As the coarse root architectures expanded from localized rooting (Sc1) to more extensive rooting (Sc3), relative carbon costs for coarse roots increased as a function of tree size, with the extensively rooted trees investing upwards of nine-fold more towards lateral structure compared to the localized scenario (Fig. 10b). These differences are most pronounced in large growth trees (DBH>25cm, Large cluster) which make up more than two-thirds the canopy crown volume (Fig. 10c).

Expansion of the root system increases the size of an individual's soil water reservoir but benefits to water uptake can be dampened by increased interactions with neighboring roots, so that the actual useable water volume may not keep pace with increases in root system volume (Fig. 10d). While increasing lateral spread alleviates constrained uptake (the cost of cooperation, W, becomes smaller), to a degree, individuals are still unable to meet the full atmospheric demand (W is larger than zero). Despite large investments in structural carbon for the *large*

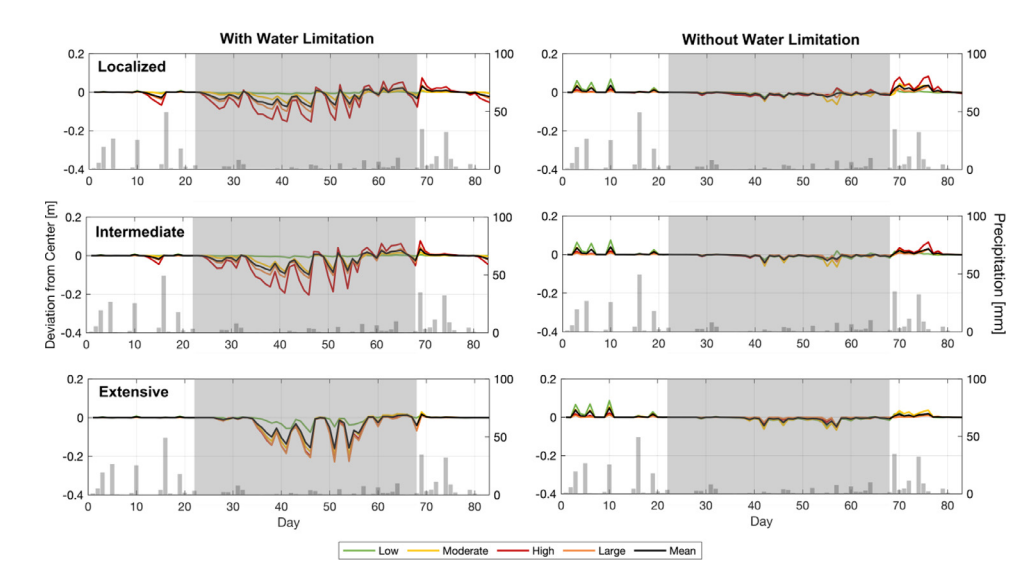


Fig. 7. (Left panel) The shift of the weighted centroid of water uptake away from the center of root mass distribution (0.385 m) for Soil 1 for the three interaction scenarios. (Right panel) The shift of the weighted centroid of uptake away from the center of mass for Soil 2 for the same interaction scenarios. In all plots, interaction groups are given by the legend, legend, gray bars are daily precipitation (mm), and the shaded gray is the observed "dry period".

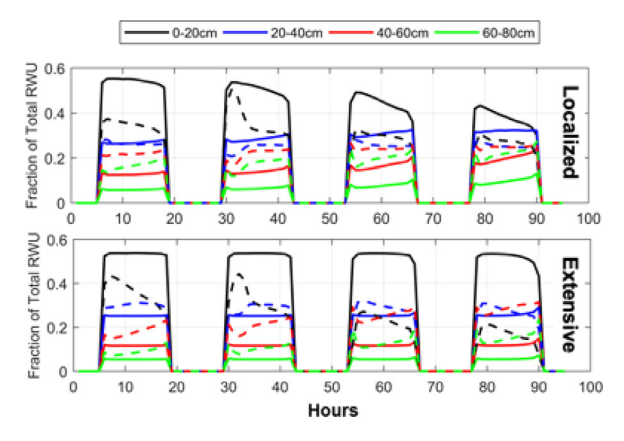


Fig. 8. The relative contribution of the various soil layers (see the legend) to domain scale water uptake for (top panel) *localized* (Sc1) and (bottom panel) *extensive* (Sc3) rooting scenarios. The simulation results for the characteristic wet period is denoted with the solid lines and for the characteristic dry period with the dashed lines. The results correspond to Soil 1.

tree and high interaction groups, water benefit (e.g., alleviation of water stress) is not gained, with *W* reaching a lower limit. Low and moderate interaction groups, with relatively low competitive pressures compared to their peers, are able to meet atmospheric demand (*W* close to zero) while maintaining low relative carbon costs.

5. Discussion

5.1. Root processes and soil moisture patterns

Root water uptake plays an important role in the spatiotemporal evolution of soil moisture, but the driving mechanisms (e.g., growth, hydraulics, distribution, etc.) underlying these patterns are not fully understood (see summary by Koch et al., 2019). The three lateral spread scenarios presented help elucidate the contribution of rooting distributions and competition on soil water content and plant water sourcing. The results further show the intimate connection between root and soil hydraulics. While derived from the same soil textural information and observed field conditions, the two soil hydraulic parameterizations show two different water regimes: one soil hydraulic parameterization inducing water limitation and the other not. While the subsequent discussion focuses primarily on the water-limiting case, it is worth noting that these responses are highly dependent on soil hydraulic properties.

As shallow soil layers (0-30cm) are depleted of water, plant water sourcing shifts to deeper soil layers (Fig. 7, left panel). When soil water is sufficient, as in Soil 2 (Table 2), all groups are able to fulfill their water demands, showing little evidence of deviation of the centroid of uptake away from the center of mass (Fig 7, right panel). The intensity, frequency, and duration of these shifts are the combined effects individual water demands and local competition. The intensity of downward shifts in water sourcing are largely driven by root system overlap and interaction. In the localized rooting scenario (Sc1), the low and moderate interaction groups (Fig. 7, left panel, green and yellow lines) have relatively exclusive access to their soil water reserves, meeting their modest atmospheric demands and averting extreme drying from shallow layers. Water uptake occurs across the entire root profile, illustrated by no deviation of the centroid of uptake from the center of mass. As lateral spreads increase and water reserves become shared among root networks, low and moderate individuals experience enhanced shallow soil drying, shifting their overall uptake to deeper soil layers. The high interaction group (Fig. 7, left panel, red lines) maintains shared soil water reservoirs across the lateral rooting scenarios, but as root lateral spreads become extensive, the magnitude or intensity of centroid deviations become greater. While the intensity of centroid shifts is greater for extensive root systems, this is offset by differences in frequency and duration. The onset of deeper water uptake, while not as strong, occurs sooner (upwards of 10 days) for localized root systems. This is primarily limited to large trees and those with moderate or high interaction. Lateral expansion of these root systems not only decreases the frequency of these shifts but increases overall uptake due to soil reservoir increases (Fig. 6 c-d).

Across the rooting scenarios, spatial patterns of soil moisture closely track root spatial distributions, becoming more homogeneous as roots expand laterally (Fig. 9). For a given soil medium, the homogenization of soil moisture represents a minimization of the free energy of the system. Heterogeneous fields contain sharp soil water potential gradients and unutilized pockets of moisture. In their thermodynamic assessment of RWU, Hildebrandt et al. (2016) demonstrated that homogeneous soil water potentials minimize energy dissipation losses during water transport delaying the onset of water limitation compared to heterogeneous conditions. This implies that in environments prone to water-limiting soil drying, a root distribution which promotes homogeneity is a thermodynamically favorable means of delaying the onset of physiological water stress. While maintaining the same amount of overall fine root length between scenarios, the coefficient of variation for the extensive systems (Cv_{Sc3}) decreased upwards of 50-70% during the mid-season dry period while cumulative transpiration increased 26% over localized roots (Cv_{Sc1}). The modeled homogeneous distribution of

% Total Crown Volume

30

20

10

0

Low Moderate High

Large

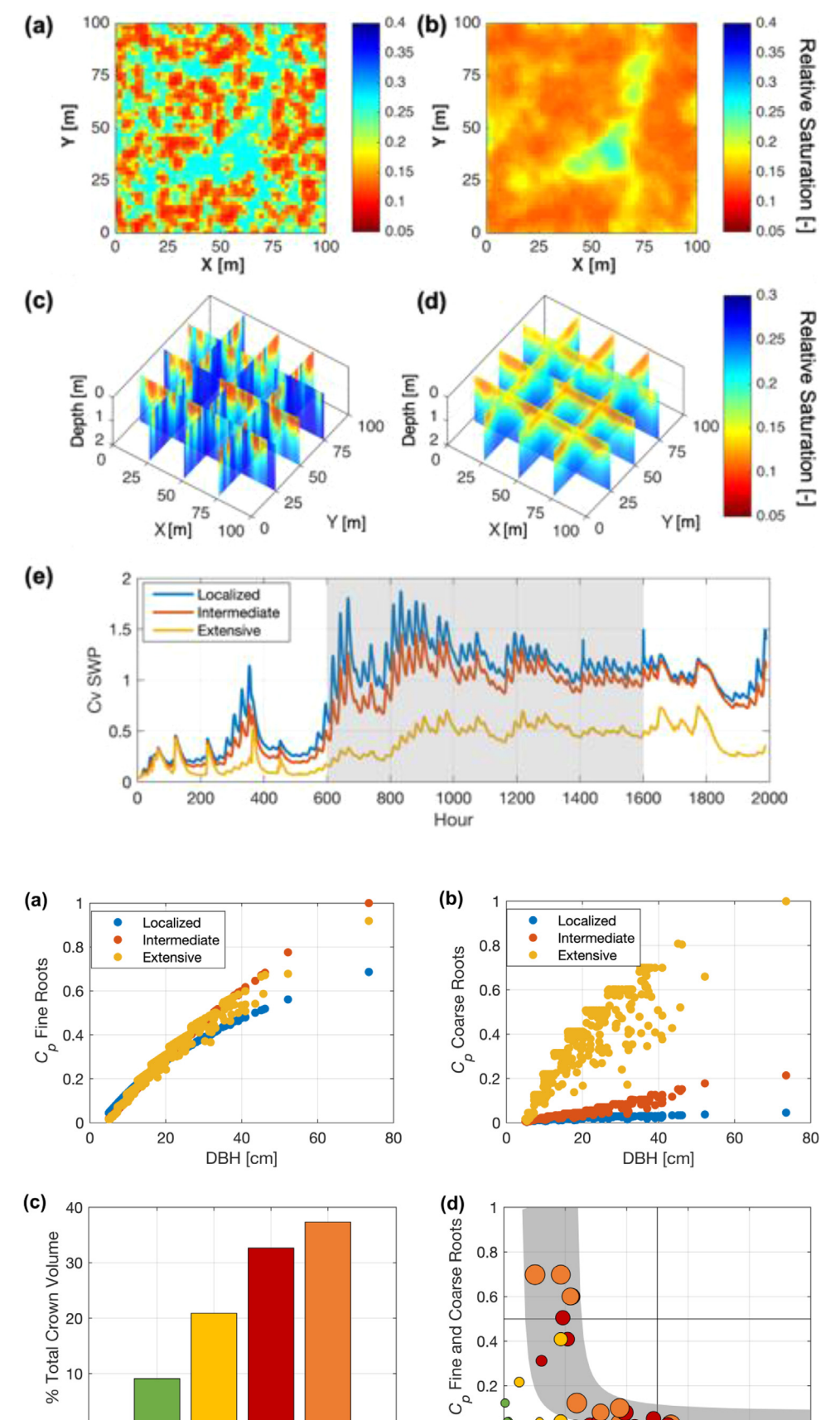


Fig. 9. (a - b) Mean relative saturation, averaged across the dry period, for the localized and extensive scenarios respectively at 2m x 2m scale. (c-d) Mean relative saturation, averaged across the dry period, for the localized and extensive scenarios at 0.05m scale. (e) Time series of spatial coefficient of variation for soil water potential across the simulated period, with dry period indicated as shaded gray.

Fig. 10. (a) The relative carbon cost of fine roots for all three scenarios of lateral expansion. (b) The relative carbon cost of coarse root architecture for all three scenarios of lateral expansion. (c) Relative crown volume of each representative group. (d) The relative structural $cost(C_p)$ versus the ability to meet atmospheric demand or the cost of cooperation, W_p , under Soil 1 for the four representative groups. The gray shaded region encompasses the majority of trees as illustrated by (c).

0.4

0.6

 W_p

8.0

0.2

0.8

0.6

0.4

0.2

soil water of the *extensive* roots (Sc3) contributed to a more homogeneous soil water potential field, and subsequently higher rates of water uptake.

Further consequences of large soil water potential gradients may include the cavitation of root xylem vessels or physical separation of fine roots from the soil, decreasing the conductance of water from the soil into the plant. Within the leaf, decline of water conductance has been shown to begin in outside-xylem vessels, a mechanism suggested to mitigate the effect of increasing xylem tensions that may lead to cavitation of water transport vessels (Scoffoni et al., 2017). Within the rhizosphere, the shrinkage of roots promotes a disconnection from soils (Carminati et al., 2009), separating the rhizosphere from highly negative soil water potentials. The ability of roots to dynamically adjust their region of uptake due to this decoupling is an important strategy to ameliorate the potentially physiologically detrimental effects of dry soils (Carminati and Vetterlein, 2013).

5.2. The carbon cost and water benefit of exploration

As roots extend laterally or down through soil layers, individuals incur a greater overall carbon cost, both from tissue construction and subsequent respiratory maintenance (Fig. 10a-b). This growth increases the size of an individual's soil water reservoir but benefits to water uptake can be dampened by increased interactions with neighboring roots, so that the actual useable water volume may not keep pace with increases in root system volume. As such, water benefits from carbon investment depend largely on forest density and tree size (e.g., relative competition and demand), but reach a threshold upon which further benefit cannot be gained by expansion (Fig. 10d).

The four presented interaction groups - low, moderate, and high interaction, and large tree - provide a point of comparison for how relative competition and atmospheric demands for water generate independent pressures for root system segregation or expansion. Low and moderate interaction groups have low relative competition and demand and are analogous to young or low density forest stands. These groups perform well with localized lateral roots (Sc1), able to nearly or fully meet their atmospheric demand without the need for extensive exploration (Figs. 6a, 10d). This is not the case for individuals in denser stand areas (high interaction) or with large atmospheric demands (large trees). Large trees, with DBH>25 cm (Fig. 5b), constrain uptake more often and earlier than smaller trees with similar relative competition (similar RCI), unable to meet their proportionately larger atmospheric demands. High interaction root systems also experience the impacts of water limitation more strongly than other groups (Fig. 6b-d, 10d). Extensive lateral rooting (Sc3) reduces the number of 'soil controlled' days for these groups, improving their overall performance. Though expansion does not fully alleviate water stress for these groups, it suggests that as forests become denser or larger, more extensive root structures confer a water acquisition benefit despite increases in root competition (greater RCI). The low interaction group, composed of smaller trees with relatively lower demand, benefits most from horizontal segregation (i.e., the lateral isolation of the root system from competitors), while larger trees with higher demands must forego segregation in order to meet their larger water demands, particularly during times of low precipitation. Exclusive soil water access is a benefit only while soil water reservoirs are sufficient to meet demand.

It is expected that in the space of costs and benefits resulting from the imposed root spatial exploration, there should be an optimal or "viable" region of co-existence. In this region, access to a larger soil reservoir has the benefit of water stress alleviation (i.e., *W* reduction, even when competing for soil water with other individuals) and results in "justifiable" carbon costs up to a point, after which further investments in rooting spread do not provide additional water uptake benefits. This is expected to be particularly true for individuals with *high interaction* or *large* size. Despite having high relative carbon costs (Fig. 10a, d), additional water benefit reaches a lower limit, as seen from the lack of reduction in

W (Fig. 10d). Beyond this threshold, carbon investment or allocation is best channeled towards other means of drought response.

An alternative viable strategy to ameliorate drought stress is to access deeper soil water. Deep rooting has long been proposed as a coping mechanism for water limitation in some species (e.g., Barbeta et al., 2015; Nepstad et al., 1994; Thomsen et al., 2013). This study instituted a uniform rooting depth of 80 cm, a depth which encompasses a majority of the fine root profile (as evidenced by field data), to isolate the impact of lateral spread. Within this limit, mean soil water content in deep soil layers (≥ 1 m) remained greater than $0.10 \text{m}^3 \text{ m}^{-3}$ across the simulated period. Observations from US-UMB show dry deep soil layers, with soils from 1 to 3m maintaining moisture close to residual saturation $(0.03-0.04\text{m}^3\text{ m}^{-3})$ for the majority of the growing season (Fig 1b). Our results indirectly support empirical evidence from the same study site of deep water uptake during periods of infrequent precipitation. In Matheny et al. (2014), deep-rooted red oaks (Quercus rubra) were able to meet atmospheric demand during dry periods, while shallow-rooted red maples (Acer rubrum) were not. The different rooting-depth strategies of these two species were confirmed using xylem water isotope analysis (Matheny et al., 2017a). To cope with water limitation, individuals experiencing high atmospheric demand and those with high competitive pressure or lateral interaction must optimize both lateral spread and rooting depth to maintain water uptake during dry periods. Our analysis supports empirical studies that highlight the importance of both tree size and spatial proximity as determinants of stable plant water relations during drought (Lechuga et al., 2018).

5.3. Representation of root structure and their coupling with stem and canopies in models

Implementation of interacting root system structure and RWU in terrestrial models is an area of opportunity for large scale terrestrial models (Warren et al., 2015). Three-dimensional representation of individual root architecture requires substantial data for parameterization and validation, operating within a limited data space compared to analogous above-ground properties. The simulations here used best available data for community structure, soil conditions, and species-specific hydraulic properties within the study area (Supplemental Material S3). Despite scant information about below-ground structure and function, valuable insights are gained by coupling root hydraulic architecture and interaction with models that capture soil water dynamics. One- and quasi two-dimensional representations of root profiles have offered insights into how forest below-ground structure can help sustain transpiration during dry periods by fully utilizing different zones of available moisture (e.g., Ivanov et al., 2012). Expanding upon these insights, we have shown that lateral interaction and competition between root systems plays a quantifiable role in plant water sourcing. The four representative groups showed divergent behavior in their response to water limitation in terms of zones of uptake and ability to meet potential demand. Individuals of the same size, but with different degrees of interaction, responded differently, with higher degrees of interaction driving water uptake into deeper soil layers.

Assigning hydraulic properties and atmospheric demand by species would be a future avenue of research and may further elucidate the complex interplay of plant hydraulic strategies at the individual and community scale. Representative groups were determined as a function of their size and degree of competitive interaction. Hydraulic strategy serves as a potential third axis for determining representative groups, either within pre-existing plant functional types that are utilized by most earth system models or as a novel paradigm to define plant groupings on a more physical basis (Matheny et al. 2017b). Here we neglected stem hydraulic resistance, though it may become substantial in tall cavitating trees. A simplistic "beam" hydraulics such as plant functional types that are utilized by most earth system models accounting for vertical variations of sapwood geometry and hydraulic traits (Couvreur et al., 2018) or more detailed stem architecture and capacitance model

(Mirfenderesgi et al., 2016; Bohrer et al., 2005) could be implemented in future versions, and would allow more realistic feedbacks between cavitation and leaf regulation of transpiration (Bartlett et al., 2016). For this numerical exercise, net precipitation was distributed uniformly across the domain, decoupling soil moisture patterns generated from root processes from those generated by precipitation throughfall. Guswa et al. (2012) demonstrated that horizontal variability in soil moisture is modulated in space and time by root (e.g., hydraulic redistribution and compensatory water uptake) and canopy processes (e.g., interception and stemflow). As such, incorporating heterogeneous precipitation would be an avenue of future research.

The current generation of dynamic global vegetation models (DGVMs) has made tremendous strides in the representation of above ground canopy structure, with several modes of representation that allow for testing of hypotheses that address the dynamics among individuals or cohorts in their acquisition of light and other resources (Fisher et al., 2018). Further refinement of below-ground structure, especially in the horizontal dimension, is urgently needed to represent spatial and temporal niches of soil environment and control on vegetation function. These improvements need to have mechanistic coupling with more fully resolved soil hydraulics to provide the critical basis for linkage between below- and above-ground processes needed to address questions of resource acquisition, carbon allocation, and relevant tradeoffs.

6. Conclusions

In this work, we presented a coupled three-dimensional model of soil water dynamics and root water uptake that utilizes a hybrid macroscale approach to represent three-dimensional root hydraulic architecture. This model was used to examine the role of root lateral interactions on root water uptake processes and plant water sourcing under waterlimiting conditions. Spatial root distributions and the degree of lateral interaction between root systems is shown to shape the spatiotemporal evolution of soil moisture, with interaction contributing to the shift of water uptake to deeper soil horizons during periods of low precipitation. Exploration of the root system, through expansion of lateral roots, results in the homogenization of soil water potentials, a thermodynamically favorable condition which also helps delay the onset of water limitation. However, root lateral expansion comes with higher carbon investment cost in root tissue production and maintenance, suggesting that an optimal or viable region exists which balances resource acquisition needs with investments in structure. This work further demonstrates that lateral or horizontal interactions are a critical dimension to consider when examining ecosystem water relations, especially under conditions of water limitation.

Supplemental information

The PFLOTRAN-Root model repository is available as an open source public release (DOI: 10.5281/zenodo.3540881). Model input files and parameterizations generated for this study are publicly available (DOI: 10.5281/zenodo.4270139).

Declaration of Competing Interest

The authors declare that they have no known competing financial interests or personal relationships that could have appeared to influence the work reported in this paper.

CRediT authorship contribution statement

Elizabeth Agee: Methodology, Investigation, Formal analysis, Data curtion, Writing – original draft, Visualization, Writing – review & editing. **Lingli He:** Conceptualization, Software, Writing – review & editing.

Gautam Bisht: Software, Writing – review & editing. Valentin Couvreur: Methodology, Software, Writing – review & editing. Parisa Shahbaz: Data curtion, Writing – review & editing. Félicien Meunier: Software, Writing – review & editing. Christopher M. Gough: Data curtion, Formal analysis, Writing – review & editing. Ashley M. Matheny: Data curtion, Formal analysis, Writing – review & editing. Gil Bohrer: Data curtion, Formal analysis, Writing – review & editing. Valeriy Ivanov: Data curtion, Formal analysis, Supervision, Funding acquisition, Writing – review & editing.

Acknowledgements

E. Agee and V. Ivanov acknowledge the partial support from DOE award DE-SC0011078, NSF DEB awards 1754163, 09111444, 0911461, NSF OPP award 1725654, NASA Earth and Space Science Fellowship Program award 17-EARTH17F-84, and the J.B. and Marilyn McKenzie Graduate Endowment Fund at the University of Michigan Biological Station. This material is based upon work supported by the U.S. Department of Energy, Office of Science, Office of Biological and Environmental Research under contract number DE-AC05-00OR22725. Funding for meteorological and flux data collection in the US-UMB AmeriFlux core site was provided by the U.S. Department of Energy's Office of Science. V. Couvreur was supported by Postdoctoral grants from the FNRS (1208619F), the Interuniversity Attraction Poles Programme-Belgian Science Policy (grant IAP7/29), and the "Communauté française de Belgique-Actions de Recherches Concertées" (grants ARC11/16-036 and ARC16/21-075). G. Bisht was supported by the Energy Exascale Earth System Model (E3SM) project, funded by the U.S. Department of Energy, Office of Science, Office of Biological and Environmental Research). C. Gough was supported by National Science Foundation Division of Environmental Biology Award 1655095. G. Bohrer and A. Matheny were supported by NSF award 1521238. During prepartion of this manuscript, F. Meunier was funded by the BAEF and the WBI as a research fellow and then by the FWO as a junior postdoc (grant 1214720N). The authors appreciate the support of the University of Michigan Biological Station staff, especially C. Vogel.

Supplementary materials

Supplementary material associated with this article can be found, in the online version, at doi:10.1016/j.advwatres.2021.103896.

References

Allen, C.D., Macalady, A.K., Chenchouni, H., Bachelet, D., McDowell, N., Vennetier, M., et al., 2010. A global overview of drought and heat-induced tree mortality reveals emerging climate change risks for forests. Forest Ecol. Manag. 259 (4), 660–684. https://doi.org/10.1016/j.foreco.2009.09.001.

Anderegg, W.R.L., Klein, T., Bartlett, M., Sack, L., Pellegrini, A.F.A., Choat, B., Jansen, S, 2016. Meta-analysis reveals that hydraulic traits explain cross-species patterns of drought-induced tree mortality across the globe. *Proc. Natl. Acad. Sci.* 113 (18), 5024–5029. https://doi.org/10.1073/pnas.1525678113.

Arney, J.D., 1973. Tables for Quantifying Competitive Stress on Individual Trees (Inf Report No. BC-X-78) (p. 10). Pacific Forest Research Centre: Canadian Forestry Service.

Baram, S., Couvreur, V., Harter, T., Read, M., Brown, P.H., Kandelous, M., Smart, D.R., Hopmans, J.W, 2016. Estimating Nitrate leaching to groundwater from Orchards: comparing crop nitrogen excess, deep vadose zone data-driven estimates, and HY-DRUS modeling. *Vadose Zone J.* 15 (11). https://doi.org/10.2136/vzj2016.07.0061.

Barbeta, A., Mejía-Chang, M., Ogaya, R., Voltas, J., Dawson, T.E., Peñuelas, J., 2015. The combined effects of a long-term experimental drought and an extreme drought on the use of plant-water sources in a Mediterranean forest. *Global Change Biol.* 21 (3), 1213–1225. https://doi.org/10.1111/gcb.12785.

Bartlett, M.K., Klein, T., Jansen, S., Choat, B., Sack, L., 2016. The correlations and sequence of plant stomatal, hydraulic, and wilting responses to drought. PNAS 113 (46), 13098– 13103. https://doi.org/10.1073/pnas.1604088113.

Bloom, A.J., Chapin, F.S., 1985. Resource limitation in plants-an economic analogy. Annu. Rev. Ecol. System. 16, 363–392.

Bohrer, G., Mourad, H., Laursen, T.A., Drewry, D., Avissar, R., Poggi, D., Oren, R., Katul, G., 2005. Finite element tree crown hydrodynamics model (FETCH) using porous media flow within branching elements: a new representation of tree hydrodynamics. *Water Resour. Res.* 41 (11). https://doi.org/10.1029/2005WR004181.

Brum, M., Vadeboncoeur, M.A., Ivanov, V., Asbjornsen, H., Saleska, S., Alves, L.F., et al., 2018. Hydrological niche segregation defines forest structure and

- drought tolerance strategies in a seasonal Amazon forest. *J. Ecol.* 107 (1). https://doi.org/10.1111/1365-2745.13022.
- Cai, G., Vanderborght, J., Couvreur, V., Mboh, C.M, Vereecken, H., 2018. Parameterization of root water uptake models considering dynamic root distributions and water uptake compensation. *Vadose Zone J.* 17 (1), 160125. https://doi.org/10.2136/vzj2016.12.0125.
- Canham, 2005. GLI Ray Analyzer Retrieved from http://www.sortie-nd.org/other_downloads/GLI_Ray_Analyzer_Help/help.html .
- Carminati, A., Vetterlein, D., Weller, U., Vogel, H., Oswald, S.E, 2009. When roots lose contact. Vadose Zone J. 8 (3), 805–809. https://doi.org/10.2136/vzj2008.0147.
- Carminati, Andrea, Vetterlein, Doris, 2013. Plasticity of rhizosphere hydraulic properties as a key for efficient utilization of scarce resources. Ann. Bot. (Lond.) 112 (2), 277– 290. https://doi.org/10.1093/aob/mcs262.
- Casper, B.B., Schenk, H.J., Jackson, R.B., 2003. Defining a plant's belowground zone of influence. *Ecology* 84 (9), 2313–2321. https://doi.org/10.1890/02-0287.
- Ciais, P., Reichstein, M., Viovy, N., Granier, A., Ogée, J., Allard, V., et al., 2005. Europe-wide reduction in primary productivity caused by the heat and drought in 2003. Nature 437 (7058), 529–533. https://doi.org/10.1038/nature03972.
- Couvreur, V., Vanderborght, J., Javaux, M., 2012. A simple three-dimensional macroscopic root water uptake model based on the hydraulic architecture approach. *Hydrol. Earth Syst. Sci.* 16 (8), 2957–2971. https://doi.org/10.5194/hess-16-2957-2012.
- Couvreur, V., Vanderborght, J., Draye, X., Javaux, M., 2014. Dynamic aspects of soil water availability for isohydric plants: focus on root hydraulic resistances. *Water Resour. Res.* 50 (11), 8891–8906. https://doi.org/10.1002/2014WR015608.
- Couvreur, V., Ledder, G., Manzoni, S., Way, D.A., Muller, E.B., Russo, S.E., 2018. Water transport through tall trees: a vertically explicit, analytical model of xylem hydraulic conductance in stems. *Plant, Cell Environ.* 41 (8), 1821–1839. https://doi.org/10.1111/pce.13322.
- Doussan, C., Pierret, A., Garrigues, E., Pagès, L., 2006. Water uptake by plant roots: II—modelling of water transfer in the soil root-system with explicit account of flow within the root system—comparison with experiments. *Plant Soil* 283 (1–2), 99–117. https://doi.org/10.1007/s11104-004-7904-z.
- Fatichi, S., Katul, G.G., Ivanov, V.Y., Pappas, C., Paschalis, A., Consolo, A., et al., 2015a. Abiotic and biotic controls of soil moisture spatiotemporal variability and the occurrence of hysteresis. Water Resour. Res. 51 (5), 3505–3524. https://doi.org/10.1002/2014WR016102.
- Fatichi, S., Pappas, C., Ivanov, V.Y., 2015b. Modeling plant-water interactions: an ecohydrological overview from the cell to the global scale. Wiley Interdiscip. Rev.: Water https://doi.org/10.1002/wat2.1125.
- Fisher, R.A., Koven, C.D., Anderegg, W.R.L., Christoffersen, B.O., Dietze, M.C., Farrior, C.E., Holm, J., et al., 2018. Vegetation demographics in earth system models: a review of progress and priorities. Global Change Biol. 24 (1), 35–54. https://doi.org/10.1111/gcb.13910.
- Garrity, S.R., Meyer, K., Maurer, K.D., Hardiman, B., Bohrer, G., 2012. Estimating plot-level tree structure in a deciduous forest by combining allometric equations, spatial wavelet analysis and airborne LiDAR. Remote Sens. Lett. 3 (5), 443–451. https://doi.org/10.1080/01431161.2011.618814.
- Guswa, A.J., 2008. The influence of climate on root depth: a carbon cost-benefit analysis. Water Resour. Res. 44 (2). https://doi.org/10.1029/2007WR006384.
- Guswa, A.J., 2012. Canopy vs. roots: production and destruction of variability in soil moisture and hydrologic fluxes. *Vadose Zone J.* 11 (3). https://doi.org/10.2136/vzj2011.0159.
- Hammond, G.E., Lichtner, P.C., Mills, R.T., 2014. Evaluating the performance of parallel subsurface simulators: an illustrative example with PFLOTRAN: Evaluating the Parallel Performance of Pflotran. Water Resour. Res. 50 (1), 208–228. https://doi.org/10.1002/2012WR013483.
- He, L., Ivanov, V.Y., Bohrer, G., Thomsen, J.E., Vogel, C.S., Moghaddam, M., 2013. Temporal dynamics of soil moisture in a northern temperate mixed successional forest after a prescribed intermediate disturbance. *Agric. For. Meteorol.* 180, 22–33. https://doi.org/10.1016/j.agrformet.2013.04.014.
- He, L., Ivanov, V.Y., Bohrer, G., Maurer, K.D., Vogel, C.S., Moghaddam, M., 2014. Effects of fine-scale soil moisture and canopy heterogeneity on energy and water fluxes in a northern temperate mixed forest. *Agric. For. Meteorol.* 184, 243–256. https://doi.org/10.1016/j.agrformet.2013.10.006.
- Hildebrandt, A., Kleidon, A., Bechmann, M., 2016. A thermodynamic formulation of root water uptake. Hydrol. Earth Syst. Sci. 20 (8), 3441–3454. https://doi.org/10.5194/hess-20-3441-2016.
- Ivanov, V.Y., et al., 2008. Vegetation-hydrology dynamics in complex terrain of semiarid areas: 1. A mechanistic approach to modeling dynamic feedbacks: Modeling vegetation-hydrology feedbacks. Water Resour. Res. 44 (3). https://doi.org/10.1029/2006WR005588.
- Ivanov, V.Y., Fatichi, S., Jenerette, G.D., Espeleta, J.F., Troch, P.A., Huxman, T.E., 2010. Hysteresis of soil moisture spatial heterogeneity and the "homogenizing" effect of vegetation: soil moisture spatial heterogeneity. Water Resour. Res. 46 (9). https://doi.org/10.1029/2009WR008611.
- Ivanov, V.Y., Hutyra, L.R., Wofsy, S.C., Munger, J.W., Saleska, S.R., de Oliveira, R.C., de Camargo, P.B., 2012. Root niche separation can explain avoidance of seasonal drought stress and vulnerability of overstory trees to extended drought in a mature Amazonian forest: root niche separation as drought avoidance strategy. Water Resour. Res. 48 (12). https://doi.org/10.1029/2012WR011972.
- Javaux, M., Couvreur, V., Vanderborght, J., Vereecken, H., 2013. Root water uptake: from three-dimensional biophysical processes to macroscopic modeling approaches. *Vadose Zone J.* 12 (4). https://doi.org/10.2136/vzj2013.02.0042, 0.
- Koch, A., Meunier, F., Vereecken, H., Javaux, J. 2019. Root processes affecting soil moisture patterns in ecohydrology. In: Li, X., Vereecken, H. (Eds.), Observation and Mea-

- surement of Ecohydrological Processes. Springer, Berlin, Heidelberg, pp. 417–433. https://doi.org/10.1007/978-3-662-48297-1_13 edited byEcohydrology.
- Kolb, T.E., Fettig, C.J., Ayres, M.P., Bentz, B.J., Hicke, J.A., Mathiasen, R., et al., 2016. Observed and anticipated impacts of drought on forest insects and diseases in the United States. Forest Ecol. Manag. 380, 321–334. https://doi.org/10.1016/j.foreco.2016.04.051.
- Kramer-Walter, K.R., Bellingham, P.J., Millar, T.R., Smissen, R.D., Richardson, S.J., Laughlin, D.C., 2016. Root traits are multidimensional: specific root length is independent from root tissue density and the plant economic spectrum. *J. Ecol.* 104 (5), 1299–1310. https://doi.org/10.1111/1365-2745.12562.
- Lang, C., Dolynska, A., Finkeldey, R., Polle, A., 2010. Are beech (Fagus sylvatica) roots territorial? Forest Ecol. Manag. 260 (7), 1212–1217. https://doi.org/10.1016/j.foreco.2010.07.014.
- Lechuga, V., Carraro, V., Viñegla, B., Carreira, J.A., Linares, J.C., 2018. Reprint of "managing drought-sensitive forests under global change. Low competition enhances long-term growth and water uptake in Abies pinsapo. Forest Ecol. Manag. 418, 23–33. https://doi.org/10.1016/j.foreco.2017.11.038.
- Leitner, D., Klepsch, S., Bodner, G., Schnepf, A., 2010. A dynamic root system growth model based on L-Systems. *Plant Soil* 332 (1–2), 177–192. https://doi.org/10.1007/s11104-010-0284-7.
- Leuschner, C., Hertel, D., Coners, H., Büttner, V., 2001. Root competition between beech and oak: a hypothesis. *Oecologia* 126 (2), 276–284. https://doi.org/10.1007/s004420000507.
- Lichtner, P.C., Hammond, G.E., Lu, C., Karra, S., Bisht, G., Andre, B., et al., 2017. PFLOTRAN User Manual.
- Littell, J.S., Peterson, D.L., Riley, K.L., Liu, Y., Luce, C.H., 2016. A review of the relationships between drought and forest fire in the United States. *Global Change Biol.* 22 (7), 2353–2369. https://doi.org/10.1111/gcb.13275.
- Lloyd, S.P., 1982. Least squares quantization in pcm. IEEE Trans. Inf. Theory 28, 129–137.
 Makita, N., Hirano, Y., Dannoura, M., Kominami, Y., Mizoguchi, T., Ishii, H., Kanazawa, Y.,
 2009. Fine root morphological traits determine variation in root respiration of Quercus serrata. Tree Physiol. 29 (4), 579–585. https://doi.org/10.1093/treephys/tpn050.
- Manoli, G., Bonetti, S., Domec, J.-C., Putti, M., Katul, G., Marani, M., 2014. Tree root systems competing for soil moisture in a 3D soil-plant model. Adv. Water Res. 66, 32-42. https://doi.org/10.1016/j.advwatres.2014.01.006.
- Matheny, A.M., et al., 2014. Species-specific transpiration responses to intermediate disturbance in a Northern Hardwood forest. J. Geophys. Res. Biogeosci. 119 (12), 2014JG002804. https://doi.org/10.1002/2014JG002804.
- Matheny, A.M., Fiorella, R.P., Bohrer, G., Poulsen, C.J., Morin, T.H., Wunderlich, A., et al., 2017a. Contrasting strategies of hydraulic control in two codominant temperate tree species. Ecohydrology 10 (3), e1815. https://doi.org/10.1002/eco.1815.
- Matheny, A.M., Mirfenderesgi, G., Bohrer, G., 2017b. Trait-based representation of hydrological functional properties of plants in weather and ecosystem models. Plant Diversity 39 (1), 1–12.
- Meunier, F., Draye, X., Vanderborght, J., Javaux, M., Couvreur, V., 2017.
 A hybrid analytical-numerical method for solving water flow equations in root hydraulic architectures. Appl. Math. Modell. 52, 648–663. https://doi.org/10.1016/j.apm.2017.08.011.
- Mirfenderesgi, G., Bohrer, G., Matheny, A.M., Fatichi, S., Frasson, R., Schäfer, K.V.R., 2016. Tree level hydrodynamic approach for resolving aboveground water storage and stomatal conductance and modeling the effects of tree hydraulic strategy. J. Geophys. Res.: Biogeosciences 121 (7), 1792–1813. https://doi.org/10.1002/2016JG003467.
- Mualem, Yechezkel, 1976. A new model for predicting the hydraulic conductivity of unsaturated porous media. Water Resour. Res. 12 (3), 513–522. https://doi.org/10.1029/WR012i003p00513.
- McCormack, M.L., Guo, D., Iversen, C.M., Chen, W., Eissenstat, D.M., Fernandez, C.W., et al., 2017. Building a better foundation: improving root-trait measurements to understand and model plant and ecosystem processes. *New Phytol.* 215 (1), 27–37. https://doi.org/10.1111/nph.14459.
- McDowell, N.G., Fisher, R.A., Xu, C., Domec, J.C., Hölttä, T., Mackay, D.S., et al., 2013. Evaluating theories of drought-induced vegetation mortality using a multimodel-experiment framework. New Phytol. 200 (2), 304–321. https://doi.org/10.1111/nph.12465.
- Meinen, C., Leuschner, C., Ryan, N.T., Hertel, D., 2009. No evidence of spatial root system segregation and elevated fine root biomass in multi-species temperate broad-leaved forests. Trees 23 (5), 941–950. https://doi.org/10.1007/s00468-009-0336-x.
- Montagnoli, A., Terzaghi, M., Di Iorio, A., Scippa, G.S., Chiatante, D., 2012. Fine-root morphological and growth traits in a Turkey-oak stand in relation to seasonal changes in soil moisture in the Southern Apennines, Italy. *Ecol. Res.* 27 (6), 1015–1025. https://doi.org/10.1007/s11284-012-0981-1.
- Nave, L.E., Gough, C.M., Maurer, K.D., Bohrer, G., Hardiman, B.S., Moine, J.L., et al., 2011. Disturbance and the resilience of coupled carbon and nitrogen cycling in a north temperate forest. J. Geophys. Res.: Biogeosciences (G4) 116. Retrieved from https://agupubs.onlinelibrary.wiley.com/doi/abs/10.1029/2011JG001758.
- Nepstad, D.C., Carvalho, C.R.de, Davidson, E.A., Jipp, P.H., Lefebvre, P.A., Negreiros, G.H., et al., 1994. The role of deep roots in the hydrological and carbon cycles of Amazonian forests and pastures. *Nature* 372 (6507), 666-669. https://doi.org/10.1038/372666a0.
- Pastorello, G., Trotta, C., Canfora, E., Chu, H., Christianson, D., Cheah, Y.-W., et al., 2020. The FLUXNET2015 dataset and the ONEFlux processing pipeline for eddy covariance data. Sci. Data 7 (1), 225. https://doi.org/10.1038/s41597-020-0534-3.

- Phillips, R.P., Ibáñez, I., D'Orangeville, L., Hanson, P.J., Ryan, M.G., McDowell, N.G., 2016. A belowground perspective on the drought sensitivity of forests: towards improved understanding and simulation. Forest Ecol. Manag. 380, 309–320. https://doi.org/10.1016/j.foreco.2016.08.043.
- Preisler, H.K., Grulke, N.E., Heath, Z., Smith, S.L., 2017. Analysis and out-year forecast of beetle, borer, and drought-induced tree mortality in California. Forest Ecol. Manag. 399, 166–178. https://doi.org/10.1016/j.foreco.2017.05.039.
- Rajkai, K., Várallyay, G., 1992. Estimating soil water retention from simpler properties by regression techniques. In: Proc. Int. Workshop on Indirect Methods for Estimating the Hydraulic Properties of Unsaturated Soils. University of California, Riverside, pp. 417–426.
- Rewald, B., Leuschner, C., 2009. Belowground competition in a broad-leaved temperate mixed forest: pattern analysis and experiments in a four-species stand. Eur. J. For. Res. 128 (4), 387–398. https://doi.org/10.1007/s10342-009-0276-4.
- Richards, L.A., 1931. Capillary conduction of liquids through porous mediums. Physics 1 (5), 318–333. https://doi.org/10.1063/1.1745010.
- Richardson, L.F., 1922. Weather Prediction by Numerical Process. Cambridge University Press, Cambridge.
- Schenk, H.J., Callaway, R.M., Mahall, B.E., 1999. Spatial root segregation: are plants territorial? In: Fitter, A.H., Raffaelli, D. (Eds.) Advances in Ecological Research, 28. Academic Press, pp. 145–180. https://doi.org/10.1016/S0065-2504(08)60032-X.
- Schlesinger, W.H., Dietze, M.C., Jackson, R.B., Phillips, R.P., Rhoades, C.C., Rustad, L.E., Vose, J.M., 2016. Forest biogeochemistry in response to drought. *Global Change Biol*. 22 (7), 2318–2328. https://doi.org/10.1111/gcb.13105.
- Schymanski, S.J., Sivapalan, M., Roderick, M.L., Beringer, J., Hutley, L.B., 2008. An optimality-based model of the coupled soil moisture and root dynamics. *Hydrol. Earth Syst. Sci.* 12 (3), 913–932. https://doi.org/10.5194/hess-12-913-2008.
- Scoffoni, C., Albuquerque, C., Brodersen, C.R., Townes, S.V., John, G.P, Bartlett, M.K., Buckley, T.N., McElrone, A.J., Sack, L., 2017. Outside-xylem vulnerability, not xylem embolism, controls leaf hydraulic decline during dehydration. *Plant Physiol.* 173 (2), 1197–1210. https://doi.org/10.1104/pp.16.01643.
- Silvertown, J., Araya, Y., Gowing, D., 2015. Hydrological niches in terrestrial plant communities: a review. J. Ecol. 103 (1), 93–108. https://doi.org/10.1111/1365-2745.12332.

- Stone, E.L., Kalisz, P.J., 1991. On the maximum extent of tree roots. *Forest Ecol. Manag.* 46, 59–102.
- Sulis, M., Couvreur, V., Keune, J., Cai, G., Trebs, I., Junk, J., et al., 2019. In-corporating a root water uptake model based on the hydraulic architecture approach in terrestrial systems simulations. *Agric. For. Meteorol.* 269–270, 28–45. https://doi.org/10.1016/j.agrformet.2019.01.034.
- Sutton, R.F., Tinus, R.W., 1983. Root and root system terminology. Forest Sci. 29 (suppl_1), a0001–z0001. https://doi.org/10.1093/forestscience/29.s1.a0001.
- Thomsen, J.E., Bohrer, G., Matheny, A.M., Ivanov, V.Y., He, L., Renninger, H.J., Schäfer, K.V.R, 2013. Contrasting hydraulic strategies during dry soil conditions in Quercus rubra and Acer rubrum in a sandy site in Michigan. Forests 4 (4), 1106– 1120. https://doi.org/10.3390/f4041106.
- Valverde-Barrantes, O.J., Smemo, K.A., Feinstein, L.M., Kershner, M.W., Blackwood, C.B., 2015. The distribution of below-ground traits is explained by intrinsic species differences and intraspecific plasticity in response to root neighbours. J. Ecol. 101 (4), 933–942. https://doi.org/10.1111/1365-2745.12087.
- van Genuchten, M.T., 1980. A closed-form equation for predicting the hydraulic conductivity of unsaturated soils. Soil Sci. Soc. Am. J. 44 (5), 892–898. https://doi.org/10.2136/sssai1980.03615995004400050002x.
- Warren, J.M., Hanson, P.J., Iversen, C.M., Kumar, J., Walker, A.P., Wullschleger, S.D., 2015. Root structural and functional dynamics in terrestrial biosphere models - evaluation and recommendations. *New Phytol.* 205 (1), 59–78. https://doi.org/10.1111/nph.13034.
- Weemstra, M., Mommer, L., Visser, E.J.W., van Ruijven, J., Kuyper, T.W., Mohren, G.M.J., Sterck, F.J, 2016. Towards a multidimensional root trait framework: a tree root review. New Phytol. 211 (4), 1159–1169. https://doi.org/10.1111/nph.14003.
- Yang, Y., Donohue, R.J., McVicar, T.R., 2016. Global estimation of effective plant rooting depth: implications for hydrological modeling. Water Resour. Res. 52 (10), 8260–8276. https://doi.org/10.1002/2016WR019392.
- Zhao, M., Running, S.W., 2010. Drought-Induced reduction in global terrestrial net primary production from 2000 through 2009. Science 329 (5994), 940–943. https://doi.org/10.1126/science.1192666.